The Astrophysical Journal, 872:195 (7pp), 2019 February 20 https://doi.org/10.3847/1538-4357/ab0108

1-OGC: The First Open Gravitational-wave Catalog of Binary Mergers from Analysis of Public Advanced LIGO Data

Alexander H. Nitz[1,2], Collin Capano[1,2], Alex B. Nielsen[1,2], Steven Reyes[3], Rebecca White[3,4], Duncan A. Brown[3], and Badri Krishnan[1,2]
[1] Max-Planck-Institut für Gravitationsphysik (Albert-Einstein-Institut), D-30167 Hannover, Germany; alex.nitz@aei.mpg.de
[2] Leibniz Universität Hannover, D-30167 Hannover, Germany
[3] Department of Physics, Syracuse University, Syracuse, NY 13244, USA
[4] Fayetteville-Manlius High School, Manlius, NY 13104, USA
Received 2018 November 6; revised 2019 January 18; accepted 2019 January 21; published 2019 February 25

Abstract

We present the first Open Gravitational-wave Catalog, obtained by using the public data from Advanced LIGO's first observing run to search for compact-object binary mergers. Our analysis is based on new methods that improve the separation between signals and noise in matched-filter searches for gravitational waves from the merger of compact objects. The three most significant signals in our catalog correspond to the binary black hole mergers GW150914, GW151226, and LVT151012. We assume a common population of binary black holes for these three signals by defining a region of parameter space that is consistent with these events. Under this assumption, we find that LVT151012 has a 97.6% probability of being astrophysical in origin. No other significant binary black hole candidates are found, nor did we observe any significant binary neutron star or neutron star–black hole candidates. We make available our complete catalog of events, including the subthreshold population of candidates.

Key words: black hole physics – gravitational waves – stars: neutron

1. Introduction

The Advanced LIGO gravitational-wave observatories (Abbott et al. 2016g) performed their first observing run (O1) from 2015 September 12 to 2016 January 19. This provided a total of 51.5 days of coincident observations from the two detectors located in Hanford, WA and Livingston, LA. The binary black hole (BBH) mergers observed in this observing run have been reported by the LIGO and Virgo Collaborations (LVC) in Abbott et al. (2016a, 2016d, 2016e). These BBH detections have been independently studied by Green & Moffat (2018), Roulet & Zaldarriaga (2019), and Antelis & Moreno (2018).

Since the publication of the results by Abbott et al. (2016a, 2016i), improvements to the data-analysis methods used (Abbott et al. 2016c) have been implemented (Dal Canton & Harry 2017; Nitz et al. 2017; Nitz 2018). Using these improvements, we re-analyze the O1 data and provide—for the first time—a full catalog of candidate events from a matched-filter search for compact-binary coalescences using the O1 data, which we call 1-OGC. This catalog provides estimates of the significance of previously known events and a ranked list of subthreshold candidates. Although not significant by themselves, these subthreshold candidates can be correlated with archival data or transient events found by other astronomical observatories to provide constraints on the population of compact-object mergers (Ashton et al. 2018; Burns et al. 2018).

Our catalog is based entirely on public, open data and software. We use the LIGO data available from the Gravitational Wave Open Science Center (Vallisneri et al. 2015) and analyze the data using the open-source PyCBC toolkit (Dal Canton et al. 2014; Usman et al. 2016; Nitz et al. 2018c).This toolkit was also used by one of the two analyses described in Abbott et al. (2016c). The lowest-mass sources targeted in our search are neutron star binaries with total mass $m_1 + m_2 = 2\,M_\odot$. The search space extends to BBH systems that produce gravitational waveforms longer than 0.15 s from 20 Hz. This corresponds to a total mass up to $500\,M_\odot$ for sources with high mass ratios and spins where the component aligned with the orbital angular momentum is positive and large. For binaries with negligible spin, this corresponds to total mass $\lesssim 200\,M_\odot$. The search space also includes neutron star–black hole binaries. After applying cuts for data quality (Abbott et al. 2016b, 2018), a total of 48.1 days of coincident data are searched for signals.

The three most significant signals in the catalog correspond to GW150914 (Abbott et al. 2016e), LVT151012 (Abbott et al. 2016a, 2016e), and GW151226 (Abbott et al. 2016d), respectively. No other astrophysically significant signals are observed. In the analysis of Abbott et al. (2016a), LVT151012 was the third-most significant event, but it was not sufficiently significant to be labeled as an unambiguous detection. With the improved methods employed here, the false alarm rate (FAR) of this candidate improves by an order of magnitude and it should be considered a true astrophysical event. The analyses of Abbott et al. (2016a, 2016i) restricted the astrophysical search space to binaries with a total mass less that $100\,M_\odot$. Our analysis extends this target space to higher-mass signals. No additional signals are detected in this region of parameter space, consistent with the results of Abbott et al. (2017g).

A second observing run (O2) of the Advanced LIGO detectors took place from 2016 November 30 to 2017 August 25 (Abbott et al. 2016f). The Virgo gravitational-wave detector also collected data for part of this period, starting from 2017 August 1. The detections reported in this second observing run thus far include three additional BBH coalescence events (Abbott et al. 2017b, 2017d, 2017e) and a binary neutron star

merger (Abbott et al. 2017a). However, the full O2 data set has not yet been released. The catalog presented here is therefore restricted to the first observing run, O1.

Our paper is organized as follows: In Sections 2 and 3, we summarize our analysis methods, including the parameter space searched, the detection statistic used for ranking candidate events, and our method for calculating the statistical significance of events. The search results are summarized in Section 4. Our full catalog and released data are described in Section 5 and are available online as supplementary materials.[5] In this paper, we focus on the detection of compact objects. Since no new astrophysical events have been observed, we do not consider measurement of the signals' parameters and refer to Abbott et al. (2016a) and Biwer et al. (2019) for discussion of the detected events' source-frame properties. Consequently, we quote binary mass parameters in the detector frame in this work.

2. Search Methodology

To search for gravitational waves from compact-object mergers, we use matched filtering (Allen et al. 2012) implemented in the open-source PyCBC library (Dal Canton et al. 2014; Usman et al. 2016; Nitz et al. 2018c). Our methods improve on the analyses of Abbott et al. (2016a, 2016c, 2016i) by imposing a phase, amplitude, and time delay consistency on candidate signals; an improved background model; and a larger search parameter space (Dal Canton & Harry 2017; Nitz et al. 2017; Nitz 2018).

2.1. Target Search Space

A discrete bank of gravitational-wave template waveforms (Owen 1996; Owen & Sathyaprakash 1999; Brown et al. 2012) is used to target binary neutron star, neutron star–black hole, and BBH mergers with total mass from 2 to 500 $M_\odot$ (Dal Canton & Harry 2017). The templates are parameterized by their component masses $m_{1,2}$ and their dimensionless spins $\boldsymbol{\chi}_{1,2} = c\boldsymbol{S}_{1,2}/Gm_{1,2}^2$, where $\boldsymbol{S}_{1,2}$ are the spin vectors of each compact object. For compact objects with component masses greater than 2 $M_\odot$, the template bank covers a wide range of spins, with $\chi_{(1,2)z} \in [\pm 0.998]$, where $\chi_{(1,2)z}$ are the components aligned with the orbital angular momentum. For compact objects with masses less than 2 $M_\odot$, the spin is restricted to $\chi_{(1,2)z} \in [\pm 0.05]$ (Brown et al. 2012). Templates that correspond to sources with a signal duration less than 0.15 s (starting from 20 Hz) are excluded due to the difficulty in separating candidates arising from these templates from populations of instrumental glitches (Dal Canton & Harry 2017). Consequently, the total mass boundary of the search depends strongly on the "effective spin" (Racine 2008; Ajith et al. 2011),

$$\chi_{\rm eff} = \frac{\chi_{1z} m_1 + \chi_{2z} m_2}{m_1 + m_2}. \quad (1)$$

This dependence is visible in the distribution of the approximately 400,000 templates required to cover the space shown in Figure 1. A dotted line in Figure 1 denotes the upper boundary of the O1 analysis performed in Abbott et al. (2016a). For binaries with total mass greater than 4 $M_\odot$, we use the spinning effective-one-body model (SEOBNRv4; Taracchini et al. 2014; Bohé et al. 2016) as template gravitational waveforms. For sources with total masses less than 4 $M_\odot$ we use TaylorF2 post-Newtonian waveforms with phasing accurate to 3.5 post-Newtonian order and the dominant amplitude evolution (Sathyaprakash & Dhurandhar 1991; Droz et al. 1999; Blanchet 2002; Faye et al. 2012). Our choice of template bank discretization causes less than a 10% loss in detection rate for any source within the boundaries of the template bank. Our search assumes that the source can be adequately described by only the dominant gravitational-wave mode, two component masses, non-precessing spins, and negligible eccentricity.

2.2. Creation and Ranking of Candidate Events

For each template and each detector, we calculate the matched-filter signal-to-noise ratio (S/N) as a function of time $\rho(t)$ (Allen et al. 2012). The template bank is divided into 15 equal sized subbanks based on the chirp mass $\mathcal{M} = (m_1 m_2)^{3/5}/(m_1 + m_2)^{1/5}$ of each template. A single-detector "trigger" is a peak in the S/N time series that is greater than 4 and larger than any other peaks within 1 s. For each subbank, the loudest 100 triggers (by ρ) are recorded in ~1 s fixed time windows. This method has been shown to improve search sensitivity, while making the rate of single-detector triggers manageable (Nitz et al. 2018b). We have found this choice of subbanks to be an effective method to ensure the analysis can concurrently record triggers from separate regions of parameter space that respond differently to instrumental noise. Other choices are possible.

We use the data-quality segments provided by the Gravitational Wave Open Science Center to exclude triggers that occur in times when there are problems with the detectors' data quality (Abbott et al. 2016b, 2018). In addition, very loud transient glitches, corresponding to $>100\sigma$ deviations from Gaussian noise, are excised from the strain data according to the procedure of Usman et al. (2016) before calculation of the S/N time series. However, there remain many types of transient non-Gaussian noise in the LIGO data that produce triggers with large values of S/N (Nuttall et al. 2015; Abbott et al. 2016b, 2018).

For every trigger with $\rho > 5.5$ we calculate the signal consistency test, χ_r^2, introduced in Allen (2005). The statistic χ_r^2 divides the matched filter into frequency bands and checks that the contribution from each band is consistent with the expected signal. The statistic takes values close to unity when the data contain either Gaussian noise or the expected signal and larger values for many types of transient glitches. We impose the S/N limit as the χ_r^2 test is generally noninformative when $\rho < 5.5$. The χ_r^2 value is used to re-weight the S/N ρ as (Babak et al. 2013)

$$\tilde{\rho} = \begin{cases} \rho & \text{for } \chi_r^2 \leqslant 1 \\ \rho \left[\frac{1}{2}(1 + (\chi_r^2)^3)\right]^{-1/6}, & \text{for } \chi_r^2 > 1. \end{cases} \quad (2)$$

For single-detector triggers from templates with total mass greater than 40 $M_\odot$ we apply an additional test, $\chi_{r,\rm sg}^2$, that determines if the detector output contains power at higher frequencies than the maximum expected frequency content of the gravitational-wave signal (Nitz 2018). This test is only applied for higher-mass systems, since these templates are shorter in duration and more difficult to separate from instrumental noise. For other systems, we set $\chi_{r,\rm sg}^2 = 1$. Using

[5] https://github.com/gwastro/1-ogc

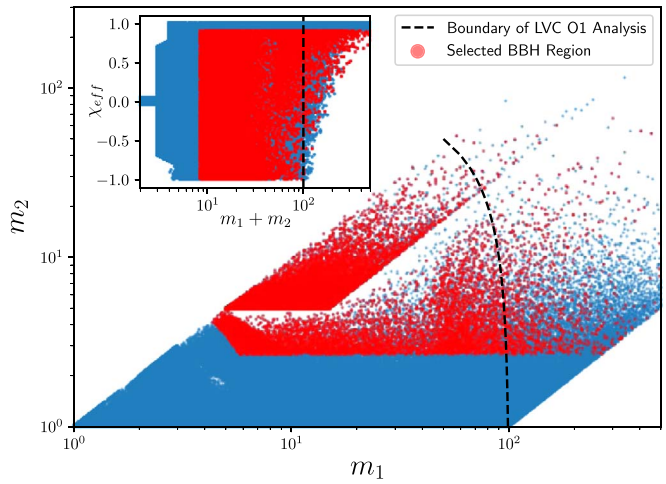

Figure 1. Component masses and spins of the templates used to search for compact-binary mergers. Due to the exclusion of short-duration templates, there is a dependency on the total mass searched and its effective spin. For binary black holes with negligible spin, this implies that this study only probes sources with total mass less than $200\,M_{\odot}$. Visible artifacts due to the procedure for constructing the template bank do not impact performance. Templates that we conservatively consider to produce binary black hole (BBH) candidates consistent with known observations are shown in red as discussed in Section 3. The upper mass boundary of the analysis performed by the LVC in Abbott et al. (2016a) is shown as a black dotted line.

this statistic, we apply a further re-weighting as

$$\hat{\rho} = \begin{cases} \tilde{\rho} & \text{for } \chi^2_{r,\mathrm{sg}} \leqslant 4 \\ \tilde{\rho}(\chi^2_{r,\mathrm{sg}}/4)^{-1/2}, & \text{for } \chi^2_{r,\mathrm{sg}} > 4. \end{cases} \tag{3}$$

Candidate events are generated when single-detector triggers occur in both the LIGO Hanford and Livingston data within 12 ms (the light-travel time between the observatories extended by 2 ms for signal time-measurement error) and if the triggers are recorded in the same template in each detector (Usman et al. 2016). Following the procedure of Nitz et al. (2017), we model the distribution of single-detector triggers from each template as an exponentially decaying function, $\lambda(\hat{\rho}, \boldsymbol{\theta}^N)$, where $\boldsymbol{\theta}^N$ allows the parameters of the exponential to vary as a function of total mass, symmetric mass ratio $\eta = m_1 m_2/M^2$, and χ_{eff}. This fitted model allows us to rescale $\hat{\rho}$ to better equalize the rate of triggers from each template.

We improve upon the ranking of candidates in Abbott et al. (2016a, 2016i) by also taking into account $p^S(\boldsymbol{\theta}^S)$, which is the expected distribution of S/N ρ_H and ρ_L, phase difference $\phi_{c,H} - \phi_{c,L}$, and arrival time delay $t_{c,H} - t_{c,L}$ between the two LIGO instruments for an astrophysical population (Nitz et al. 2017). No assumption is made about the distribution of intrinsic source parameters in this term. The primary benefit arises from assuming the population of sources is isotropically distributed in orientation and sky location. The final ranking statistic $\tilde{\rho}_c$ is then calculated as

$$\tilde{\rho}_c \propto [\log p^S(\boldsymbol{\theta}^S) - \log(\lambda_H(\hat{\rho}_H, \boldsymbol{\theta}^N)\lambda_L(\hat{\rho}_L, \boldsymbol{\theta}^N))] + \text{const.} \tag{4}$$

This expression is normalized so that $\tilde{\rho}_c$ approximates the standard network S/N $\rho_c = (\rho_L^2 + \rho_H^2)^{1/2}$ for candidates from regions of parameter space that are not affected by elevated rates of instrumental noise. Candidates from regions affected by elevated rates of noise triggers are down-weighted and assigned a smaller statistic value by this method. As multiple candidates, which arise from different template waveforms, may occur in response to the same signal, we select only the highest-ranked candidate within 10 s. A simpler version of this statistic where the single-detector exponential noise model is only a function of the template duration has also been employed in the analysis of data from LIGO's second observing run (Abbott et al. 2017c, 2017d, 2017f).

2.3. Statistical Significance

The statistical significance of candidate events is estimated by measuring empirically the rate of false alarms. To measure the noise background rate, we generate additional analyses by time shifting the data from one instrument with respect to the other by multiples of 100 ms. Since this time shift is greater than the maximum astrophysical time of flight between observatories, any candidates produced in these analyses are false alarms. This time shift is much greater than the autocorrelation length of our template waveforms of $\mathcal{O}$ (1 ms). The time-slid analyses are produced following the same procedure as the search; this is a key requirement for our analysis to produce valid statistical results (Abbott et al. 2016c). The equivalent of more than 50,000 yr of observing time can be generated from 5 days of data.

To provide an unbiased measure of the rate of false alarms at least as significant as a potential candidate, the single-detector triggers that compose the candidate event should be included in the background estimation (Capano et al. 2017). However, when a real signal with a large $\tilde{\rho}_c$ is present in the data, the rate of false alarms for candidate events with smaller $\tilde{\rho}_c$ tends to be overestimated. This is due to the fact that the loud single-detector triggers from the real event in one detector form coincidences with noise fluctuations in the other detector, producing loud coincident background events. As in Abbott et al. (2016a), an unbiased rate of false alarms can be achieved by a hierarchical procedure whereby a candidate with large $\tilde{\rho}_c$ is removed from the estimation of background for candidates with smaller $\tilde{\rho}_c$; we use this procedure here.

3. Evaluating Candidates Based on the Astrophysical Population

We find two candidate events with FAR <1 per 50,000 yr, corresponding to GW150914 and GW151226. Although FAR does not give the probability that an event is an astrophysical signal, we can be confident that these events were not caused by chance coincidence between the detectors. It is possible that these events were caused by a correlated source between the detectors. However, detailed follow-up studies of GW150914 and GW151226 found no correlated noise sources between the detectors that could be mistaken for a gravitational wave (Abbott et al. 2016b, 2016d).

We conclude that GW150914 and GW151226 are astrophysical in origin and use them to constrain the rate of real signals. A "true discovery rate" (TDR) can be constructed for less significant events. The TDR is defined as

$$\mathrm{TDR}(\tilde{\rho}_c) = \frac{\mathcal{T}(\tilde{\rho}_c)}{\mathcal{T}(\tilde{\rho}_c) + \mathcal{F}(\tilde{\rho}_c)}, \tag{5}$$

where $\mathcal{T}(\tilde{\rho}_c)$ is the rate that signals of astrophysical origin are observed with a ranking statistic $\geqslant\tilde{\rho}_c$ (the "true alarm rate") and $\mathcal{F}(\tilde{\rho}_c)$ is the FAR.

The TDR is the complement of the false discovery rate (Benjamini & Hochberg 1995) and can be used to estimate the fraction of real signals in a population. For example, if $\mathrm{TDR}(\tilde{\rho}_c) = 0.9$, it means that 90% of events with a ranking statistic $\geqslant\tilde{\rho}_c$ are expected to be real signals. The TDR is also independent of the observation time.

Note that TDR is not the probability that a particular event is a signal of astrophysical origin P_{astro}. For that, one needs to model the distribution of signals and noise at a given $\tilde{\rho}_c$. In this work, we use a simple model of these distributions as a function of the ranking statistic $\tilde{\rho}_c$. Models incorporating additional parameters are also possible, but we do not consider them here. As a function of $\tilde{\rho}_c$, P_{astro} can be computed as

$$P_{\mathrm{astro}}(\tilde{\rho}_c) = \frac{\Lambda_S P_S(\tilde{\rho}_c)}{\Lambda_S P_S(\tilde{\rho}_c) + \Lambda_N P_N(\tilde{\rho}_c)}, \tag{6}$$

where $P_S(\tilde{\rho}_c)$ and $P_N(\tilde{\rho}_c)$ are the probabilities of an event having ranking statistic $\tilde{\rho}_c$ given the signal and noise hypotheses, respectively (Guglielmetti et al. 2009; Farr et al. 2015; Abbott et al. 2016h). Λ_S and Λ_N are the rates of signal and noise events.

Since no binary neutron star or neutron star–black hole candidates are obtained from a search of the O1 data, here we restrict the calculation of both the TDR and P_{astro} to BBH observations. We include signals with total mass $M \geqslant 10\,M_\odot$, mass ratio $m_1/m_2 < 5$ (where $m_1 \geqslant m_2$), and dimensionless spins $|\chi_{(1,2)z}| < 0.5$. These choices are based on a combination of what has been observed (Abbott et al. 2016a, 2017c, 2017d, 2017f) and what is expected from models of isolated binary-star evolution ("field" binaries). The mass distribution of field binaries is dependent on a number of unknown parameters, such as the metallicity of the environment (Belczynski et al. 2014). Generally, it is expected that most binaries are close to equal mass, as typically less than 1 in $\mathcal{O}(10^3)$ simulated binaries have a mass ratio >5 in models of field-binary evolution (Dominik et al. 2015). The majority of observations of nearby X-ray binaries have yielded black holes with masses greater than $5\,M_\odot$, which has led to speculation of a "mass gap" between 3 and $5\,M_\odot$ (Ozel et al. 2010; Farr et al. 2011; Kreidberg et al. 2012). The signals detected so far by LIGO and Virgo are consistent with this: the smaller component mass in the lowest-mass system known to date, GW170608, has an estimated mass of $7^{+2}_{-2}\,M_\odot$ (Abbott et al. 2017d).

The spin distribution of black holes is not well constrained (Reynolds 2014). The component spins of the most significant BBHs detected by LIGO and Virgo are only weakly constrained (Abbott et al. 2016a). The best measured quantity related to spin is χ_{eff}. All of the BBH gravitational-wave signals detected so far have $|\chi_{\mathrm{eff}}| \lesssim 0.2$. A binary with low χ_{eff} may still have component masses with large spin magnitudes, if the spins are antiparallel or are purely in the plane of the binary. However, it seems unlikely that this would be the case for all of the detections made so far. Hence, we include signals that have component spins with $|\chi_{(1,2)z}| < 0.5$. This is consistent with recent population synthesis models, which indicate that black holes must have low natal spin in order to obtain a distribution of χ_{eff} that satisfies gravitational-wave observations (Belczynski et al. 2017; Wysocki et al. 2018).

To estimate the rate and distribution of false alarms that arise only from the region consistent with this selected population of BBH mergers, we must determine which templates are sensitive to these sources. It is necessary to analyze a simulated set of signals as the template associated with a particular event is not guaranteed to share the true source parameters. We find that the region of the template bank defined by $M > 8.5\,M_\odot$, $m_{1,2} > 2.7\,M_\odot$, and $\chi_{\mathrm{eff}} < 0.9$ is effective at recovering this population of sources. This region is shown in Figure 1 in red.

To estimate the true rate $\mathcal{T}$, we use the two significant events observed during O1, GW150914, and GW151226. We do not use any of the O2 events because the full data are not yet available for analysis, making it difficult to obtain a consistent rate estimate. The total analysis time in O1 was ∼48 days, giving $\mathcal{T} \approx 15\ \mathrm{yr}^{-1}$. Given the uncertainty in this estimate based on only two events, we take the rate of observations as a Poisson process and choose the lower 95% bound on $\mathcal{T}$. This yields a $\mathcal{T} \approx 2.7\ \mathrm{yr}^{-1}$. For the calculation of the TDR we use this value for all events, independent of their ranking statistic. This means we likely underestimate the TDR for events quieter than GW151226 and GW150914, but this is a conservative bias.

To estimate the probability that a given event is astrophysical in origin P_{astro}, we model the distribution of signals and noise as a function of $\tilde{\rho}_c$. It is reasonable to approximate the signal probability distribution $P_S(\tilde{\rho}_c)$ as $\propto\tilde{\rho}_c^{-4}$ (Schutz 2011; Chen & Holz 2014). We normalize the signal number density $\Lambda_S P_S(\tilde{\rho}_c)$ so that the number of signals with $\tilde{\rho}_c$ greater than or equal to some threshold $\tilde{\rho}_c^\dagger$ is $\approx 2.7\ \mathrm{yr}^{-1}$. We make the conservative choice to place $\tilde{\rho}_c^\dagger$ at the value of the next largest $\tilde{\rho}_c$ value after GW150914 and GW151226.

To approximate the noise number density $\Lambda_N P_N(\tilde{\rho}_c)$, we make a histogram of the $\tilde{\rho}_c$ values of false alarms arising from our selected BBH region. We use only the false alarms that are uncorrelated with possible candidate events to ensure an unbiased estimate of the mean FAR (Capano et al. 2017). We fit an exponential decay to this histogram from $8 < \tilde{\rho}_c < 9.2$. For $\tilde{\rho}_c$ much less than 8, $\Lambda_N P_N$ is not well modeled by an exponential due to the effects of applying a threshold to single-detector triggers. We note, however, there is only a 50% chance that an event is astrophysical at $\tilde{\rho}_c \sim 8.6$, and this chance quickly becomes negligible with decreasing $\tilde{\rho}_c$. The result of this procedure is shown in Figure 2. We caution that P_{astro} for candidates with $\tilde{\rho}_c > 9.2$ will be sensitive to the form of the model chosen as it is not constrained by empirically measured false alarms.

While we do not assess the astrophysical probabilities of sources outside our selected BBH region, we are not precluding that such sources exist. Our P_{astro} is compatible with any model of the true BBH source distribution that allows for a signal rate to be at least as high as our estimate within the chosen region. This holds irrespective of whatever other kinds of sources may also be permitted.

4. Results

The results presented here are generated using the data from the first observing run of Advanced LIGO, which ran from 2015 September 12 to 2016 January 19. We divide the 16 kHz LIGO open data into nine consecutive periods of time and search each time period independently so that each analysis contains roughly five days of observing time. This time interval

Table 1
Candidate Events from the Full Search for Compact-binary Mergers in O1 Data

Designation	Julian Date	FAR^{-1}(yr)	$\tilde{\rho}_c$	ρ_H	ρ_L	m_1	m_2	$\chi_{\rm eff}$
150914+09:50:45UTC	2457279.910665	>66,000	18.45	19.67	13.38	44.21	32.16	0.09
151226+03:38:53UTC	2457382.652426	>59,000	11.62	10.73	7.43	14.83	8.50	0.24
151012+09:54:43UTC	2457307.913420	24	9.06	6.96	6.71	30.75	12.89	−0.05
151019+00:23:16UTC	2457314.516585	0.060	8.39	6.81	5.47	14.93	1.27	0.11
150928+10:49:00UTC	2457293.951122	0.042	8.37	6.05	6.34	2.53	1.02	−0.70
151218+18:30:58UTC	2457375.271929	0.029	8.24	7.11	5.38	31.29	2.35	−0.00
160103+05:48:36UTC	2457390.742504	0.026	8.22	6.01	6.60	9.75	7.29	0.49
151202+01:18:13UTC	2457358.554740	0.025	8.23	6.54	5.73	40.42	1.77	−0.26
160104+03:51:51UTC	2457391.661424	0.021	8.19	5.80	6.39	6.76	1.10	−0.51
151213+00:12:20UTC	2457369.508985	0.019	8.22	5.70	7.24	11.12	3.30	−0.79
150923+07:10:59UTC	2457288.799711	0.014	8.20	6.78	5.84	2.14	1.08	0.65
151029+13:34:39UTC	2457325.066149	0.014	8.21	6.83	5.23	2.19	1.07	−0.27
151206+14:19:29UTC	2457363.097291	0.013	8.17	5.80	6.37	100.60	1.64	0.98
151202+15:32:09UTC	2457359.147751	0.012	8.14	5.93	6.41	6.33	1.18	−0.59
151012+06:30:45UTC	2457307.771774	0.011	8.19	6.74	5.70	3.16	1.73	−0.15
151116+22:41:48UTC	2457343.446120	0.010	8.14	5.79	6.64	2.00	1.04	−0.45
151121+03:34:09UTC	2457347.649138	0.010	8.12	6.48	5.78	7.43	1.00	−0.86
150922+05:41:08UTC	2457287.737317	0.010	8.16	6.05	6.34	2.78	1.02	0.17
151008+14:09:17UTC	2457304.090202	0.008	8.16	5.84	6.10	46.38	1.19	0.38
151127+02:00:30UTC	2457353.584101	0.008	8.10	6.28	5.44	39.12	2.01	0.99

Note. Candidates are sorted by FAR evaluated for the entire bank of templates. The FAR of the top two candidates is limited only by the amount of background time estimated and only differ due to the variation in time available in their respective analyses to create background. The parameters of the template associated with each candidate are listed. Note that these are not intended as a rigorous estimation of the source parameters. Masses are given in the detector frame.

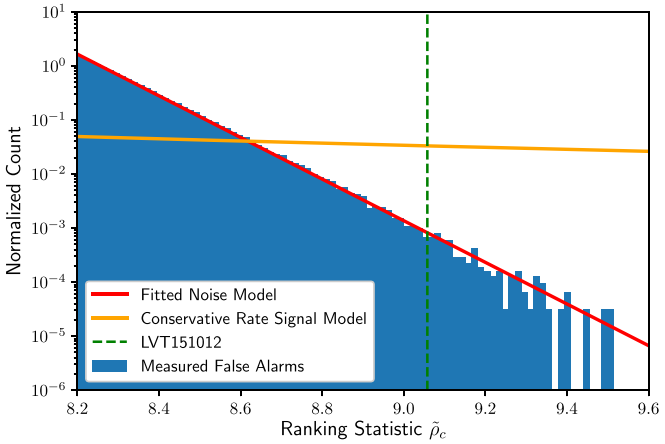

Figure 2. Scaled probability distributions of assumed signals and noise as a function of the ranking statistic $\tilde{\rho}_c$ for the analysis containing LVT151012. Blue shows the normalized histogram of empirically measured false alarms that are within our selected BBH region of the template bank, P_N. Red is the exponential decay model that has been fitted to this set of false alarms, $P_S\Lambda_S/\Lambda_N$, normalized so that the counts can be directly compared to the noise distribution. Orange shows the signal model based on our conservative rate of detections. The value of $\tilde{\rho}_c$ for LVT151012 is shown as a dotted green vertical line. The ratio of signal to noise at this value of $\tilde{\rho}_c$ strongly favors the signal model.

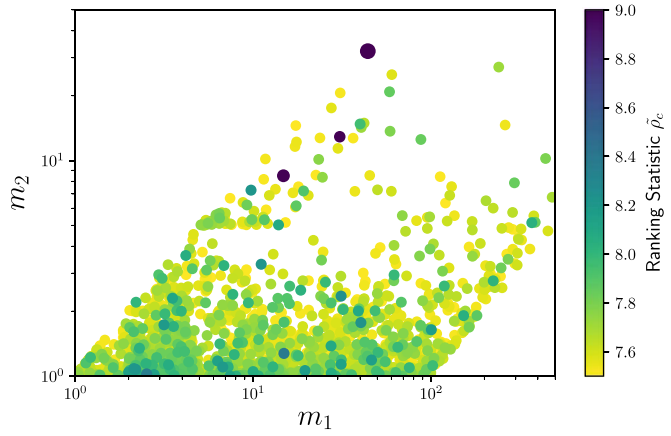

Figure 3. Candidate events with a ranking statistic $\tilde{\rho}_c > 7.5$ from the full search for compact-binary mergers in O1 data. The color bar is capped at 9. The three BBH mergers are clearly visible in the plots, while the remaining events are largely distributed according to the density of the template bank.

is set by the disk and memory requirements of the search pipeline, but it is sufficient to estimate the FAR of candidate events to better than 1 in 50,000 yr. It is possible to combine these time intervals during the analysis to improve this limit, but we have not done so here. Our analysis is restricted to times marked as observable by the metadata provided by the Gravitational Wave Open Science Center. After accounting for times that are marked as not analyzable, there remain ∼48.1 days of data when both the Hanford and Livingston LIGO instruments were operating.

The top candidate events by FAR from the full search are given in Table 1. There are three candidates that are statistically significant. These are the BBH mergers GW150914, LVT151012, and GW151226, which were previously reported in Abbott et al. (2016a, 2016d, 2016e). The FARs for GW150914 and GW151226 of 1 per 66,000 and 1 per 59,000 yr, respectively, are limits based on the amount of background time available in their respective analysis. These limits are less stringent than those reported in Abbott et al. (2016a) as we have created less background time. There are no other individually convincing candidates. Figure 3 shows candidate events with $\tilde{\rho}_c > 7.5$. The three BBH mergers stand out from the other candidate events and are clustered in a portion of the parameter space that is analyzed with relatively few template waveforms.

Table 2
Candidate Events Consistent with the Selected Population of Binary Black Holes

Designation	Julian Date	$P_{\rm astro}$	TDR	FAR^{-1}(yr)	$\tilde{\rho}_c$	ρ_H	ρ_L	m_1	m_2	$\chi_{\rm eff}$
150914+09:50:45UTC	2457279.910665	⋯	⋯	>66,000	18.45	19.67	13.38	44.21	32.16	0.09
151226+03:38:53UTC	2457382.652426	⋯	⋯	>59,000	11.62	10.73	7.43	14.83	8.50	0.24
151012+09:54:43UTC	2457307.913420	0.976	0.999	446	9.06	6.96	6.71	30.75	12.89	−0.05
160103+05:48:36UTC	2457390.742504	0.061	0.517	0.396	8.22	6.01	6.60	9.75	7.29	0.49
151213+00:12:20UTC	2457369.508985	0.047	0.455	0.309	8.22	5.70	7.24	11.12	3.30	−0.79
151216+18:49:30UTC	2457373.284799	0.017	0.223	0.106	8.09	6.10	6.01	13.92	5.03	−0.41
151222+05:28:26UTC	2457378.728506	0.012	0.169	0.075	8.03	5.67	6.46	6.86	3.26	−0.74
151217+03:47:49UTC	2457373.658627	0.006	0.088	0.036	7.96	6.69	5.57	40.02	14.77	0.84
151009+05:06:12UTC	2457304.713060	0.005	0.087	0.035	7.99	5.66	5.90	25.55	2.73	−0.05
151220+07:45:36UTC	2457376.823761	0.003	0.053	0.021	7.87	6.55	5.39	17.50	6.17	0.82
151104+04:12:55UTC	2457330.676062	0.003	0.053	0.021	7.91	5.94	6.33	19.25	7.22	0.71
151120+16:20:06UTC	2457347.181049	0.003	0.047	0.018	7.86	6.11	5.44	5.49	3.10	0.79
151216+09:24:16UTC	2457372.892271	0.003	0.045	0.017	7.86	5.76	5.66	58.56	20.84	0.66
151128+14:37:02UTC	2457355.109478	0.003	0.040	0.016	7.83	6.79	5.02	9.25	6.22	−0.87
160109+08:08:42UTC	2457396.839798	0.003	0.035	0.014	7.82	5.24	6.23	24.29	3.45	−0.98
160111+22:49:34UTC	2457399.451507	0.003	0.035	0.013	7.82	5.10	6.55	5.75	3.43	0.23
151124+11:25:19UTC	2457350.976339	0.002	0.033	0.013	7.81	5.65	6.27	98.89	3.89	0.45
150912+15:39:02UTC	2457278.152523	0.002	0.032	0.012	7.84	6.23	5.23	9.86	5.33	−0.01
151006+06:06:50UTC	2457301.755168	0.002	0.031	0.012	7.89	6.77	5.47	11.59	5.31	−0.05
151015+01:40:52UTC	2457310.570466	0.002	0.029	0.011	7.85	5.37	5.92	87.87	12.52	0.75

Note. There are three binary black hole mergers above a threshold corresponding to a true discovery rate of 99.92%. The third-most significant event, LVT151012, has a 97.6% probability of being astrophysical in origin. Note that the FARs indicated do not reflect the false alarm rate for the full search, but instead for the limited region of the template bank indicated in red in Figure 1. The FARs listed for the top two events are limited by the background time generated and so are identical to those in Table 1.

4.1. BBH Candidates

Given that there are two BBH mergers (GW150914 and GW151226) that are well established from their statistical significance, we can estimate the rate of detecting BBH mergers by this analysis. Candidate events that are consistent with our selected BBH population are listed in Table 2. We estimate the FAR of events for just this region of the analysis, and using our estimate of the true rate of detections, calculate the TDR as a function of ranking statistic. The TDR at the ranking statistic of the fourth-most significant candidate is 0.52. This means that only 52% of candidates with $\tilde{\rho}_c$ at least as large are expected to be of astrophysical origin. For each candidate we estimate its individual probability of being astrophysical in origin, $P_{\rm astro}$. The fourth event has only a 6% chance of being astrophysical. We do not report $P_{\rm astro}$ and TDR values for the top two events as these events are assumed to be signals in the construction of these statistics.

4.2. Revisiting LVT151012

LVT151012 was first announced in Abbott et al. (2016c), with a FAR of 1 per 2.3 yr. Our improved methods yield a FAR rate for LVT151012 of 1 per 24 yr. Restricting attention to our selected BBH region, which is consistent with the other observed BBH mergers, gives a FAR for LVT151012 in this region alone of 1 per 446 yr. We combine this FAR with our conservative estimate of the rate of detections to estimate that 99.92% of BBH merger candidates at least as significant as LVT151012 are astrophysical in origin. We also estimate the probability that specifically LVT151012 is astrophysical in origin to be 97.59%.

These measures both depend on our selected region of BBH sources and our estimate of the rate of true detections, but we believe our choices for both of these to be conservative. The FAR of 1 per 446 yr is not a statistical statement about the search as a whole and is used only in comparison against the rate of real signals within this same region. Selecting different boundaries for this region would yield a different FAR. However, assuming that the FAR and true alarm rate are both approximately uniform in this region, then $P_{\rm astro}$ and TDR will not change.

As data from future observing runs become available, it will be possible to more precisely estimate this rate in a consistent way and improve our estimate of this event's significance. We have modeled our signal distribution and population of false alarms as being characterized by the ranking statistic $\tilde{\rho}_c$ alone. An improved model could take into account the variation over the parameter space and in time. Figure 2 shows the probability distribution of our noise and signal models for the analysis that contains LVT151012. Compared to the $P_{\rm astro}$ reported in Abbott et al. (2016a) of 87%, our analysis has improved the ranking of candidate events, the boundaries of our selected BBH distribution differ from what was used there, and we use a more conservative estimate of the signal rate. Given a $P_{\rm astro}$ value of 97.6% we conclude that LVT151012 is astrophysical in origin. For comparison, if we had chosen the rate of observed mergers to be $\approx$15 yr^{-1}, which is the linear extrapolation of two detections in 48 days, we would find that LVT151012 had a 99.6% probability of astrophysical origin.

5. Data Release

The 1-OGC catalog contains ∼150,000 candidate events. Our supplemental materials online provide the complete combined set of binary neutron star, neutron star–black hole, and BBH candidates (Nitz et al. 2018a). A separate listing of the candidates from our selected BBH region is also made available. Each candidate is assigned an identifying name constructed from the date and UTC time. The vast majority of these candidates are not astrophysical in origin. To help

distinguish between possible sources we provide our ranking statistic $\tilde{\rho}_c$ along with our estimate of the FAR rate for each candidate. We also provide information such as the S/N observed by each instrument, the time of arrival, measured phases, and the results of our set of signal consistency tests. The periods of time that were analyzed are also provided. We also provide the PyCBC pipeline configuration files that allow our analysis to be reproduced.

6. Discussion

We present a full catalog of gravitational-wave events and candidates from a PyCBC-based, templated, matched-filter search of the LIGO O1 open data. Our analysis represents an improvement over that of Abbott et al. (2016a, 2016i) by using improved ranking of candidates by considering phase, amplitude and time delay consistency, an improved background model, and a template bank targeting a wider range of sources (Dal Canton & Harry 2017; Nitz et al. 2017; Nitz 2018). We independently verify the discovery of GW150914 and GW151226 and report an improved significance of the candidate event LVT151012, which we claim should be viewed as a confident detection. Apart from these three signals, none of the other candidate events are individually significant in our analysis. All of these candidates are listed in our catalog available at www.github.com/gwastro/1-ogc, along with tools for exploring and using it. Complete gravitational-wave event catalogs of this nature will become important tools in multimessenger astronomy.

A larger data set from the second observing run of LIGO and Virgo already exists. Individual detections have been published, and short periods of data around the detections are available publicly. However, the bulk of this data has not yet been released publicly. It will be possible to create a similar open catalog with the most up-to-date analysis tools when these data are released.

We thank Thomas Dent and Sumit Kumar for useful discussions and comments. We thank Stuart Anderson, Jonah Kannah, and Alan Weinstein for help accessing data from the Gravitational Wave Open Science Center. We acknowledge the Max Planck Gesellschaft for support and the Atlas cluster computing team at AEI Hannover. Computations were also supported by Syracuse University and NSF award OAC-1541396. D.A.B. acknowledges NSF awards PHY-1707954, OAC-1443047, and OAC-1738962 for support. S.R. acknowledges NSF award PHY-1707954 and OAC-1443047 for support. R.W. acknowledges NSF award OAC-1823378 for support. This research has made use of data, software and/or web tools obtained from the Gravitational Wave Open Science Center (https://www.gw-openscience.org), a service of LIGO Laboratory, the LIGO Scientific Collaboration and the Virgo Collaboration. LIGO is funded by the U.S. National Science Foundation. Virgo is funded by the French Centre National de Recherche Scientifique (CNRS), the Italian Istituto Nazionale della Fisica Nucleare (INFN) and the Dutch Nikhef, with contributions by Polish and Hungarian institutes.

ORCID iDs

Alexander H. Nitz https://orcid.org/0000-0002-1850-4587
Collin Capano https://orcid.org/0000-0002-0355-5998
Alex B. Nielsen https://orcid.org/0000-0001-8694-4026
Steven Reyes https://orcid.org/0000-0002-4599-6054
Rebecca White https://orcid.org/0000-0002-5192-7784
Duncan A. Brown https://orcid.org/0000-0002-9180-5765
Badri Krishnan https://orcid.org/0000-0003-3015-234X

References

Abbott, B. P., Abbott, R., Abbott, T. D., et al. 2016a, PhRvX, 6, 041015
Abbott, B. P., Abbott, R., Abbott, T. D., et al. 2016b, CQGra, 33, 134001
Abbott, B. P., Abbott, R., Abbott, T. D., et al. 2016c, PhRvD, 93, 122003
Abbott, B. P., Abbott, R., Abbott, T. D., et al. 2016d, PhRvL, 116, 241103
Abbott, B. P., Abbott, R., Abbott, T. D., et al. 2016e, PhRvL, 116, 061102
Abbott, B. P., Abbott, R., Abbott, T. D., et al. 2016f, LRR, 19, 1
Abbott, B. P., Abbott, R., Abbott, T. D., et al. 2016g, PhRvD, 93, 112004
Abbott, B. P., Abbott, R., Abbott, T. D., et al. 2016h, ApJL, 833, L1
Abbott, B. P., Abbott, R., Abbott, T. D., et al. 2016i, ApJL, 832, L21
Abbott, B. P., Abbott, R., Abbott, T. D., et al. 2017a, PhRvL, 119, 161101
Abbott, B. P., Abbott, R., Abbott, T. D., et al. 2017b, PhRvL, 118, 221101
Abbott, B. P., Abbott, R., Abbott, T. D., et al. 2017c, PhRvL, 118, 221101
Abbott, B. P., Abbott, R., Abbott, T. D., et al. 2017d, ApJL, 851, L35
Abbott, B. P., Abbott, R., Abbott, T. D., et al. 2017e, PhRvL, 119, 141101
Abbott, B. P., Abbott, R., Abbott, T. D., et al. 2017f, PhRvL, 119, 141101
Abbott, B. P., Abbott, R., Abbott, T. D., et al. 2017g, PhRvD, 96, 022001
Abbott, B. P., Abbott, R., Abbott, T. D., et al. 2018, CQGra, 35, 065010
Ajith, P., Hannam, M., Husa, S., et al. 2011, PhRvL, 106, 241101
Allen, B. 2005, PhRvD, 71, 062001
Allen, B., Anderson, W. G., Brady, P. R., Brown, D. A., & Creighton, J. D. E. 2012, PhRvD, 85, 122006
Antelis, J. M., & Moreno, C. 2018, arXiv:1807.07660
Ashton, G., Burns, E., Canton, T. D., et al. 2018, ApJ, 860, 6
Babak, S., Biswas, R., Brady, P., et al. 2013, PhRvD, 87, 024033
Belczynski, K., Buonanno, A., Cantiello, M., et al. 2014, ApJ, 789, 120
Belczynski, K., Klencki, J., Meynet, G., et al. 2017, arXiv:1706.07053
Benjamini, Y., & Hochberg, Y. 1995, J. Roy. Stat. Soc., 57, 289
Biwer, C. M., Capano, C. D., De, S., et al. 2019, PASP, 131, 024503
Blanchet, L. 2002, LRR, 5, 3
Bohé, A., Shao, L., Taracchini, A., et al. 2017, APS, 95, 044028
Brown, D. A., Harry, I., Lundgren, A., & Nitz, A. H. 2012, PhRvD, 86, 084017
Burns, E., Goldstein, A., Hui, C. M., et al. 2018, arXiv:1810.02764
Capano, C., Dent, T., Hanna, C., et al. 2017, PhRvD, 96, 082002
Chen, H.-Y., & Holz, D. E. 2014, arXiv:1409.0522
Dal Canton, T., & Harry, I. W. 2017, arXiv:1705.01845
Dal Canton, T., Nitz, A., Lundgren, A., et al. 2014, PhRvD, 90, 082004
Dominik, M., Berti, E., O'Shaughnessy, R., et al. 2015, ApJ, 806, 263
Droz, S., Knapp, D. J., Poisson, E., & Owen, B. J. 1999, PhRvD, 59, 124016
Farr, W. M., Gair, J. R., Mandel, I., & Cutler, C. 2015, PhRvD, 91, 023005
Farr, W. M., Sravan, N., Cantrell, A., et al. 2011, ApJ, 741, 103
Faye, G., Marsat, S., Blanchet, L., & Iyer, B. R. 2012, CQGra, 29, 175004
Green, M. A., & Moffat, J. W. 2018, PhL, B784, 312
Guglielmetti, F., Fischer, R., & Dose, V. 2009, MNRAS, 396, 165
Kreidberg, L., Bailyn, C. D., Farr, W. M., & Kalogera, V. 2012, ApJ, 757, 36
Nitz, A. H. 2018, CQGra, 35, 035016
Nitz, A. H., Capano, C., Nielsen, A. B., et al. 2018a, 1-OGC First Open Gravitational-wave Catalog v1.0, Zenodo, doi:10.5281/zenodo.1493357
Nitz, A. H., Dal Canton, T., Davis, D., & Reyes, S. 2018b, PhRvD, 98, 024050
Nitz, A. H., Dent, T., Dal Canton, T., Fairhurst, S., & Brown, D. A. 2017, ApJ, 849, 118
Nitz, A. H., Harry, I. W., Willis, J. L., et al. 2018c, ligo-cbc/pycbc: O2 Production Release 19, Zenodo, doi:10.5281/zenodo.596388
Nuttall, L. K., Massinger, T. J., Areeda, J., et al. 2015, CQGra, 32, 245005
Owen, B. J. 1996, PhRvD, 53, 6749
Owen, B. J., & Sathyaprakash, B. S. 1999, PhRvD, 60, 022002
Ozel, F., Psaltis, D., Narayan, R., & McClintock, J. E. 2010, ApJ, 725, 1918
Racine, E. 2008, PhRvD, 78, 044021
Reynolds, C. S. 2014, SSRv, 183, 277
Roulet, J., & Zaldarriaga, M. 2019, MNRAS, 484, 4216
Sathyaprakash, B. S., & Dhurandhar, S. V. 1991, PhRvD, 44, 3819
Schutz, B. F. 2011, CQGra, 28, 125023
Taracchini, A., Buonanno, A., Pan, Y., et al. 2014, PhRvD, 89, 061502
Usman, S. A., Nitz, A., Harry, I., et al. 2016, CQGra, 33, 215004
Vallisneri, M., Kanner, J., Williams, R., Weinstein, A., & Stephens, B. 2015, J. Phys. Conf. Ser., 610, 012021
Wysocki, D., Gerosa, D., O'Shaughnessy, R., et al. 2018, PhRvD, 97, 043014